

Detailed structural, mechanical, and electronic study of five structures for CaF_2 under high pressure

Ying Guo(郭颖), Yumeng Fang(方钰萌), and Jun Li(李俊)

Citation: Chin. Phys. B, 2021, 30 (**3**): 030502. DOI: 10.1088/1674-1056/abc67d
Journal homepage: http://cpb.iphy.ac.cn; http://iopscience.iop.org/cpb

What follows is a list of articles you may be interested in

Dynamic phase transition of ferroelectric nanotube described by a spin-1/2 transverse Ising model

Chundong Wang(王春栋), Ying Wu(吴瑛), Yulin Cao(曹喻霖), and Xinying Xue(薛新英)
Chin. Phys. B, 2021, 30 (**2**): 020504. DOI: 10.1088/1674-1056/abbbfd

Quantum quenches in the Dicke model: Thermalization and failure of the generalized Gibbs ensemble

Xiao-Qiang Su(苏晓强) and You-Quan Zhao(赵有权)
Chin. Phys. B, 2020, 29 (**12**): 120506. DOI: 10.1088/1674-1056/abc679

Fast and accurate determination of phase transition temperature via individual generalized canonical ensemble simulation

Ming-Zhe Shao(邵明哲), Yan-Ting Wang(王延颋), Xin Zhou(周昕)
Chin. Phys. B, 2020, 29 (**8**): 080505. DOI: 10.1088/1674-1056/ab9c03

Topological Anderson insulator in two-dimensional non-Hermitian systems

Hongfang Liu(刘宏芳), Zixian Su(苏子贤), Zhi-Qiang Zhang(张智强), Hua Jiang(江华)
Chin. Phys. B, 2020, 29 (**5**): 050502. DOI: 10.1088/1674-1056/ab8201

Entangled multi-knot lattice model of anyon current

Tieyan Si(司铁岩)
Chin. Phys. B, 2019, 28 (**4**): 040501. DOI: 10.1088/1674-1056/28/4/040501

Detailed structural, mechanical, and electronic study of five structures for CaF_2 under high pressure*

Ying Guo(郭颖)[1,†], Yumeng Fang(方钰萌)[1], and Jun Li(李俊)[2]

[1] *Jiangsu Collaborative Innovation Center of Atmospheric Environment and Equipment Technology, Jiangsu Key Laboratory of Big Data Analysis Technology, Nanjing University of Information Science and Technology, Nanjing* 210044, *China*
[2] *Mingde New Material Technology Co., LTD, Anji* 313300, *China*

(Received 15 August 2020; revised manuscript received 13 September 2020; accepted manuscript online 31 October 2020)

Detailed density functional theory (DFT) calculations of the structural, mechanical, thermodynamic, and electronic properties of crystalline CaF_2 with five different structures in the pressure range of 0 GPa–150 GPa are performed by both GGA (generalized gradient approximation)-PBE (Perdew–Burke–Ernzerhof) and LDA (local density approximation)-CAPZ (Cambridge Serial Total Energy Package). It is found that the enthalpy differences imply that the fluorite phase → $PbCl_2$-type phase → Ni_2In-type phase transition in CaF_2 occurs at $P_{GGA1} = 8.0$ GPa, $P_{GGA2} = 111.4$ GPa by using the XC of GGA, and $P_{LDA1} = 4.5$ GPa, $P_{LDA2} = 101.7$ GPa by LDA, respectively, which is consistent with previous experiments and theoretical conclusions. Moreover, the enthalpy differences between $PbCl_2$-type and Ni_2In-type phases in one molecular formula become very small at the pressure of about 100 GPa, indicating the possibility of coexistence of two-phase at high pressures. This may be the reason why the transition pressure of the second phase transition in other reports is so huge (68 GPa–278 GPa). The volume changed in the second phase transition are also consistent with the enthalpy difference result. Besides, the pressure dependence of mechanical and thermodynamic properties of CaF_2 is studied. It is found that the high-pressure phase of Ni_2In-type structure has better stiffness in CaF_2 crystal, and the hardness of the material has hardly changed in the second phase transition. Finally, the electronic structure of CaF_2 is also analyzed with the change of pressure. By analyzing the band gap and density of states, the large band gap indicates the CaF_2 crystal is always an insulator at 0 GPa–150 GPa.

Keywords: density functional theory (DFT), high-pressure, phase transition, coexistence

PACS: 05.70.Fh **DOI:** 10.1088/1674-1056/abc67d

1. Introduction

With the development of ultraviolet lithography technology, the calcium fluoride (CaF_2) generally becomes the focus in the semiconductor industry with its high transmittance and low absorption coefficient.[1,2] For the high laser-induced damage threshold and high transparency up to the vacuum ultra-violet (UV) area, CaF_2 can replace fused silica and has many valuable optical properties for industrial applications.[3–6] For example, it has been designated as the lens material for photolithography at wavelengths in the deep ultraviolet region.[6,7] These optical properties are due to its well-known face-centered cubic (FCC) ionic crystal structural and electronic properties, such as a very large band gap.[8–12] Besides, CaF_2 has shown an excellent internal pressure calibration in moderate high-pressure and high-temperature x-ray diffraction experiments.[13–16] Recently, the electrical transport properties of CaF_2 nanocrystals have been investigated by *in situ* impedance measurement up to 30 GPa.[17] Thus, the behaviors of its elastic properties under the influence of high pressure have attracted much attentions.[18–30]

At the pressure of 0 GPa, CaF_2 shows the cubic fluorite structure with the space group of *Fm-3m*. In 1966, Seifert found that CaF_2 can transform into a $PbCl_2$-type structure with the space group of *Pnma* under pressure 8 GPa–10 GPa.[18] Then this result was confirmed experimentally by powder diffraction in 1969.[19] Afterward, in the year of 1992, Gerward obtained the exact transition pressure of about 9.5 GPa by synchrotron radiation,[20] and the high-pressure phase is stable up to 45 GPa at 300 K. In 2002, Speziale found that transition pressure is at 8.6 GPa and 1100 K and the high-pressure phase of CaF_2 is stable up to 49 GPa at room temperature.[21,22] Then, in 2005, the phase transition in ideal hydrostatic pressure and room temperature is 8.01 GPa.[23] More importantly, Dorfman reported that CaF_2 transforms from $PbCl_2$-type structure to Ni_2In-type structure with the space group of *P63/mmc* by angled-dispersive x-ray diffraction experiments at the pressure range of 63 GPa–79 GPa in 2010.[24] Other report[25] showed some different results that the pressure-induced *Fm*3*m*–*Pnma* phase transition starts at 14.0 GPa and the orthorhombic phase is stable up to 46.5 GPa. In theories, most of the transition pressures in the first *Fm*3*m*–*Pnma* phase transition are consistent with others,[26–29] but the ones in the second *Pnma*–*P*63/*mmc* phase transition are quite different. For example, Wu reported firstly the second phase transition of CaF_2 from $PbCl_2$-type structure to Ni_2In-type structure occurs at 68 GPa–72 GPa by full-potential lin-

*Project supported by the National Natural Science Foundation of China (Grant No. 61971229).
†Corresponding author. E-mail: yguo@nuist.edu.cn
© 2021 Chinese Physical Society and IOP Publishing Ltd

earized augmented plane wave (FP-LAPW) method.[26] However, other reports predicted that the *Pnma*–*P*63/*mmc* phase transition pressures of CaF_2 are 278 GPa,[28] 105 GPa,[29] and 80 GPa,[30] respectively. Up to date, there is no unified conclusion on the changes that occurs near the second-order phase transition of CaF_2.

In this work, in order to study the performance of CaF_2 under high pressure as accurately as possible, five potential phase transition structures are researched by periodic DFT calculations with two different exchange correlations, and the structural, mechanical, thermodynamic, and electronic properties in crystal CaF_2 under hydrostatic pressure 0 GPa–150 GPa are all studied.

2. Computational details

According to the literature mentioned above, five different candidate phases of CaF_2, fluorite structure (*Fm*-3*m*, No. 225), tetragonal structure (*P*4/*mmm*, No. 123), Ni_2In-type structure (*P*6$_3$/*mmc*, No. 193), orthorhombic structure (*Pmc*2$_1$, No. 26), and $PbCl_2$-type structure (*Pnma*, No. 62), are taken into consideration. We use experimental data as the initial models of these phases. The Cambridge Serial Total Energy Package (CASTEP)[31,32] is used in all of our calculations and the plane-wave OTFG ultrasoft pseudopotentials[33,34] within the density functional theory are employed to describe the interaction between electrons and ions. In recent years, much theoretical works focused on phase transition under high pressure were done by CASTEP.[35–38] Moreover, the thermodynamic properties of CaF_2 were calculated with an approximation method on the quasi-harmonic Debye model.[39] In order to get more accurate theoretical results, two different forms of exchange–correlation (XC) energy are treated: one is generalized gradient approximation (GGA) in the Perdew–Burke–Ernzerhof (PBE)[40] functional form, and the other one is local spin density approximation (LDA) proposed by Ceperley and Alder[41] and parametrized by Perdew and Zunder[42] (CA-PZ). Besides, in the self-consistent field calculation, the density-mixing minimization method[43] and the Broyden, Fletcher, Goldfarb, and Shannon (BFGS)[44] method are used to obtain the electronic wave functions and to get the relaxed structures. After a series of convergence tests, for *Fm*-3*m*, *P*4/*mmm*, *P*6$_3$/*mmc*, *Pmc*2$_1$, and *Pnma* structures of CaF_2, we utilized the 21 × 21 × 21, 14 × 10 × 14, 21 × 21× 15, 19 × 16 × 11, and 11 × 18 × 9 *k*-points grids for the irreducible Brillouin zone, respectively, and the cutoff energy for five structures is set as 650 eV. The *k*-points and cutoff settings above ensured the band gap changed by less than 0.01 eV, so the adequate accuracy can be guaranteed. The geometry relaxation is performed by self-consistent calculations to allow the space group, cell shape, and volume to change. The total energy of the system, residual force, residual bulk stress, and displacements of atoms are converged less than 5.0×10^{-6} eV/atom, 0.01 eV/Å, 0.02 GPa, and 5.0×10^{-4} Å, respectively.

3. Result and discussion

3.1. Structural phase stability and pressure influences

It is well known that CaF_2 undergoes a second-order phase transition procedure, as fluorite structure → $PbCl_2$-type structure → Ni_2In-type structure with increasing equivalent hydrostatic pressure. In this part, to investigate phase stability and phase transitions in detail, all five possible structures (*Fm*-3*m*, *P*4/*mmm*, *P*6$_3$/*mmc*, *Pmc*2$_1$, and *Pnma* structures) of CaF_2 reported in other literature[45] were selected, and fully optimized by both GGA-PBE and LDA-CAPZ at 0 GPa as the first step. In this step, the experiments data at ambient pressure and temperature were used as input structure, and all of the ionic configurations, cell shape, and volume were allowed to change in the calculations of structural optimization. The optimized lattice parameters of five structures are listed in Table 1.

Table 1. Experimental and calculated lattice constants of CaF_2 at ambient conditions.

Phases	Space group	Lattice parameters (Å)			
		Present work		Exp.	Theo.
		GGA	LDA		
Fluorite structure	*Fm-3m*	$a=b=c=5.51$	$a=b=c=5.33$	$a=5.466$[20] $a=5.463$[46]	$a=5.5252$[26] $a=5.4872$[28] $a=5.5788$[30]
Tetragonal structure	*P*4/*mmm*	$a=b=3.7471$, $c=3.0192$	$a=b=3.6203$, $c=2.9217$	$a=b=3.735$ $c=2.867$[45]	
Ni_2In-type structure	*P*6$_3$/*mmc*	$a=b=3.8675$ $c=5.9829$	$a=b=3.7993$, $c=5.3609$		$a=3.8851$, $c=5.9267$[27] $a=3.9536$, $c=5.8751$[30]
Orthorhombic structure	*Pmc*2$_1$	$a=3.54$, $b=4.16$, $c=5.97$	$a=3.39$, $b=4.05$, $c=5.78$	$a=3.324$, $b=4.146$, $c=5.686$[45]	
$PbCl_2$-type structure	*Pnma*	$a=6.01$, $b=3.65$ $c=7.08$	$a=5.80$, $b=3.48$ $c=6.84$	$a=5.63$, $b=3.49$, $c=7.15$[20] $a=5.95$, $b=3.58$, $c=7.03$[18] $a=6.018$, $b=3.614$, $c=7.023$[22]	$a=6.0274$, $b=3.6682$, $c=7.0413$[26] $a=5.9826$, $b=3.6303$, $c=7.0499$[28] $a=5.9909$, $b=3.6025$, $c=7.0717$[29]

Overall, our results are very close to the experimental data and other calculated results, which shows the reliability of our calculation parameters. It can be seen that the results calculated with XC of GGA-PBE are slightly larger than that of LDA-CAPZ, which is caused by the effect that GGA tends to underestimate the binding energies while LDA tends to overestimate that one.

Then, to investigate the stability of CaF_2 under 0 GPa, we calculated and compared the relationship between volume and total energy of the five structures. Figure 1 shows the results calculated with GGA. The curves from the bottom represent the relationships of volume and total energy in fluorite structure, $PbCl_2$-type structure, $Pmc2_1$ structure, Ni_2In-type structure, and $P4/mmm$ structure, respectively. It means that the stable order of five structures of CaF_2 at 0 GPa is fluorite $>$ $PbCl_2$-type $>$ $Pmc2_1$ $>$ Ni_2In-type $>$ $P4/mmm$, and the fluorite structure of CaF_2 is the most stable one. This result is consistent with the experimental data and other theoretical results.[18–30]

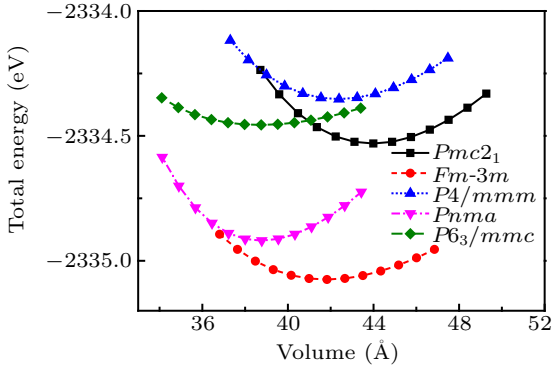


Fig. 1. Calculated energy *versus* volume per formula unit for five structures of CaF_2 at 0 GPa.

Next, to investigate the phase transitions among our selected five structures, we used the optimized structures as the input structures and calculated the Gibbs free energy G of their primitive cell. Generally, the Gibbs free energy G is[47]

$$G = E + PV - TS, \tag{1}$$

where E, P, V, T, and S are the internal energy, pressure, volume, temperature, and vibrational entropy, respectively. Since the theoretical calculations were set at $T = 0$ K, the Gibbs free energy G becomes equal to the enthalpy H

$$G = H = E + PV. \tag{2}$$

Therefore, we can get the most stable structure under one pressure by comparing the enthalpy value of different structures under that pressure. Here, we calculated the enthalpy of five different structures from 0 GPa to 150 GPa and obtained the variations curves of the enthalpy difference between fluorite structure and other four structures *versus* the pressure of CaF_2 by both GGA and LDA, which is shown in Fig. 2. Under one certain pressure, the enthalpy difference of a structure is greater than 0 indicating that the enthalpy value of this structure is greater than that of fluorite structure. So it can be seen that at lower pressure, the one with the lowest enthalpy is fluorite structure, and then $PbCl_2$-type and Ni_2In-type structures are more stable at higher pressure. As a result, the curves imply that the fluorite phase $\rightarrow$ $PbCl_2$-type phase $\rightarrow$ Ni_2In-type phase transition in CaF_2 occurs at $P_{GGA1} = 8.0$ GPa, $P_{GGA2} = 111.4$ GPa by using the XC of GGA, and $P_{LDA1} = 4.5$ GPa, $P_{LDA2} = 101.7$ GPa by LDA, respectively. These results show that the fluorite phase is the most stable structure when the pressure is below 8.0 GPa (GGA) and 4.5 GPa (LDA). Similarly, the enthalpy of Ni_2In-type structure becomes the lowest with the pressure larger than 111.4 GPa and 101.7 GPa calculated by GGA and LDA, respectively, which indicates that Ni_2In-type structure is the most stable one in the corresponding pressure ranges. Besides, the value of enthalpy in $P4/mmm$ and $Pmc2_1$ structures are always larger than the most stable structures from 0 GPa to 150 GPa, showing the instability of these two phases. Moreover, it can be seen that the enthalpy differences between $PbCl_2$-type and Ni_2In-type phases in one molecular formula become very small at the pressure of about 100 GPa, which indicate the possibility of coexistence of two-phase at high pressures.

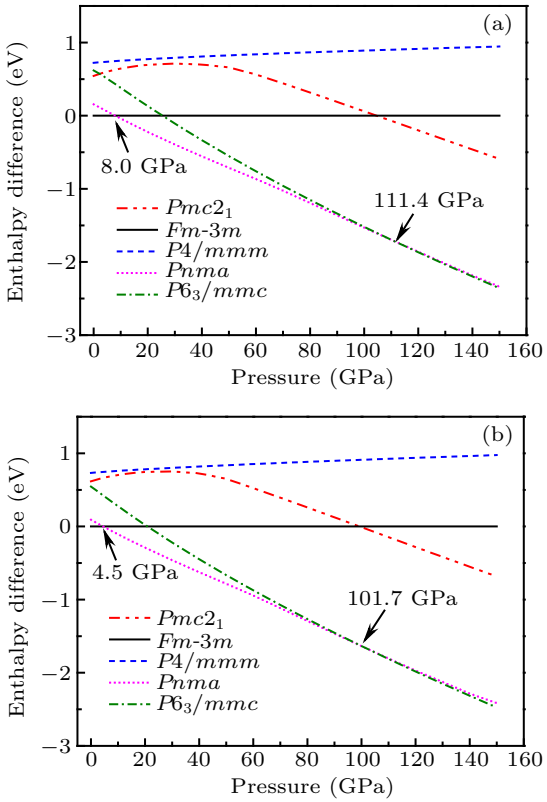


Fig. 2. Enthalpy difference between fluorite structure and other four structures as a function of pressure by (a) GGA-PBE and (b) LDA-CAPZ.

The comparisons of the transition pressures between our theoretical values and previous results are shown in Table 2. As we can see that the present result calculated with GGA (8.0 GPa) for fluorite $\rightarrow$ $PbCl_2$-type phase transition agrees well with the experimental and other theoretical transition

pressure (4.7 GPa–14 GPa). As for $PbCl_2$-type → Ni_2In-type phase transition, our results with both GGA and LDA are within other theoretical and experimental data range (68 GPa–278 GPa). We argue that the coexistence of $PbCl_2$-type and Ni_2In-type phases may be the reason why the transition pressure of the second phase transition in other reports is so huge. It is worth mentioning that the transition pressure calculated with LDA is smaller than that with GGA, which may be caused by the overestimate of the binding energy of LDA. We know that the distances between Ca^{2+} and F^- ions will close to each other with increasing pressure, and higher binding energy can accelerate the process and promote the structural transition at lower pressure.

In both $PbCl_2$-type and Ni_2In -type phase, every Ca atom has three F atoms in its nearest neighbor, and the three F atoms form a triangle with Ca atom in the middle. For example, at the pressure of phase transition (111.4 GPa), the nearest distance of Ca–F in $PbCl_2$-type phase is about 2.03 Å–2.04 Å, and the distance in Ni_2In-type phase is about 2.01 Å. Besides, the volumes of $PbCl_2$-type and Ni_2In -type phase are quite the same when the pressure is larger than about 100 GPa. These similarities in structure may cause the two phases to have similar energies under high pressure.

Table 2. The structural transition pressures from our results and other experimental and calculated data.

Data sources	Our results (GPa)		Experimental data (GPa)	Other calculated data (GPa)
	GGA	LDA		
Fluorite phase → $PbCl_2$-type phase	8.0	4.5	9.6,[20] 8.6,[21] 8.01,[23]	8,[26] 6,[26] 4.7,[48] 9.1[49]
$PbCl_2$-type phase → Ni_2In-type phase	111.4	101.7	64–79[24]	72,[26] 80,[30] 105,[29] 278[28]

In order to clarify the pressure influences on the volume of CaF_2, the changes of relative volume as a function of pressure are calculated by both GGA and LDA, and the curves are shown in Fig. 3. Generally, the volume is compressed by increasing pressure smoothly. However, at the transition pressure of fluorite to phase, the ratio of volume V/V_0 in CaF_2 changes suddenly and decreases 7.37%–8.46%, while that ratio decrease only 0.34%–0.39% at transition pressure of the $PbCl_2$-type to Ni_2In-type structure. In other words, the volume has hardly changed while the structural transition occurs between $PbCl_2$-type and Ni_2In-type phases, which is consistent with the approximately equal enthalpy of them at transition pressure, suggesting the possibility of coexistence in $PbCl_2$-type and Ni_2In-type structures.

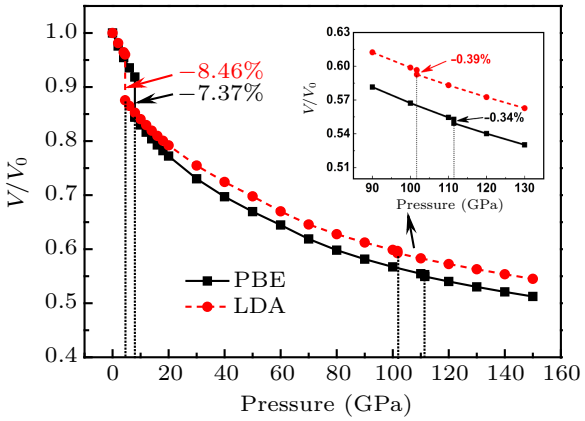


Fig. 3. Relative volume (V/V_0) as a function of pressure calculated by (a) GGA-PBE and (b) LDA-CAPZ, the inserted picture emphasizing that value from 90 GPa to 130 GPa.

In order to further investigate the pressure influences on CaF_2 and the phase transition, figure 4 shows the variations in the compression ratio of a, b, and c axes in the $PbCl_2$-type structure with increasing pressure calculated by GGA-PBE. Generally, the compression ratios for three lattice constants a/a_0, b/b_0, and c/c_0 are quite different (the "0" subscript denotes the value under the pressure of 0 GPa), indicating the compressible crystal of CaF_2 has anisotropy. Before 40 GPa, the total compressions along the a and b directions are almost the same, and smaller than that along the c direction, which means that the c axis is much stiffer than the a and b axas in the pressure range of 0 GPa–40 GPa. However, from 40 GPa to 60 GPa, the ratios of a/a_0 and c/c_0 continue to decrease, while the ratio of b/b_0 has only slight changes. Then, the compression ratio along the a direction drops quickly from 0.85 at 60 GPa to 0.77 at 80 GPa, but the ratio along the b direction at this pressure range increases from 0.90 to 0.92. Then, when the pressure is larger than 80 GPa, the ratios a/a_0 and c/c_0 decrease smoothly while b/b_0 has almost no changes. It can be understood as: at the pressure range of 60 GPa–150 GPa, the interactions between atoms is mainly concentrated in y–z plane (namely, the (1 0 0) plane), therefore, direction x (lattice parameter a) is comparatively easier to be compressed than y and z (lattice parameters b and c).

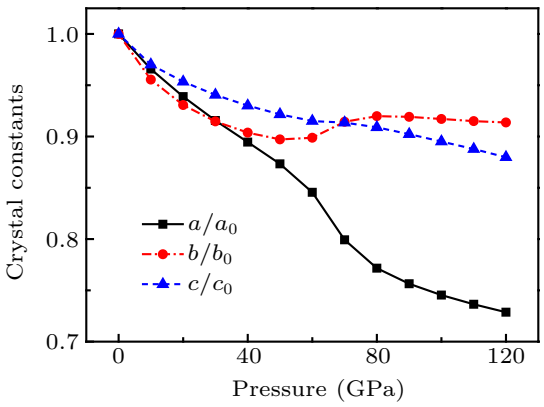


Fig. 4. Calculated crystal constants *versus* pressures for $PbCl_2$-type CaF_2 by GGA.

3.2. Mechanical and thermodynamic properties

As is known, mechanical properties can be used to certify the phase stability of the crystal at different pressures, and the elastic parameters are important indicators for analyzing mechanical properties.[50] However, researches focused on mechanical properties with increasing pressure of CaF_2 are rare in other literatures. In this part, elastic properties and mechanical moduli of five structures in CaF_2 under pressures from 0 GPa to 150 GPa are calculated with both GGA-PBE and LDA-CAPZ. Generally, the elastic constants C_{ijkl} with respect to the finite strain variables are defined as[51–53]

$$C_{ijkl} = \left.\frac{\partial \sigma_{ij}}{\partial e_{kl}}\right|_X = \frac{1}{V}\left.\frac{\partial^2 E(\chi)}{\partial \sigma_{ij}\partial e_{kl}}\right|_X, \tag{3}$$

where σ_{ij} and e_{kl} are the applied stress and Eulerian strain tensors, and χ and X are the coordinates. Although there are 21 independent components of the fourth-rank tensor C, the number will be greatly reduced with the introduction of symmetry. Taking CaF_2 for example, there are nine independent elastic constants in $Pmc2_1$ and $PbCl_2$-type phases: C_{11}, C_{22}, C_{33}, C_{12}, C_{13}, C_{23}, C_{44}, C_{55}, C_{66}, and the number of independent elastic constants in $P4/mmm$ and Ni_2In-type phases is reduced to six: $C_{11} = C_{22}$, C_{33}, C_{12}, $C_{13} = C_{23}$, $C_{44} = C_{55}$, C_{66}. However, for fluorite phase, there are only three independent elastic constants: $C_{11} = C_{22} = C_{33}$, $C_{12} = C_{13} = C_{23}$, $C_{44} = C_{55} = C_{66}$. In order to study the mechanical properties of CaF_2, we firstly calculate the elastic constants of five different phases at 0 GPa, and the results with GGA are listed in Table 3. However, the comparisons of our results with other literatures are unavailable, because the previous data are rarely reported. In addition, we can see that C_{66} in Ni_2In structure is smaller than zero, suggesting the instability of this phase at 0 GPa.

Table 1. Experimental and calculated elastic constants of five structures at 0 GPa.

	C_{11}	C_{22}	C_{33}	C_{12}	C_{13}	C_{23}	C_{44}	C_{55}	C_{66}
$Pmc2_1$ phase (our work)	115.0	127.5	137.6	23.9	13.6	74.3	35.6	15.7	15.9
$PbCl_2$ phase (our work)	131.3	101.0	113.6	37.9	47.5	34.0	13.2	24.4	40.7
1-10 $P4/mmm$ phase (our work)	156.7		211.2	45.7	13.8		11.7		51.1
Ni_2In phase (our work)	73.3		44.6	183.6	42.4		36.9		–55.2
Fluorite phase (our work)	153.4			38.8			29.1		

Table 4. Elastic constants C_{ij} of CaF_2 under various pressures 0 GPa–150 GPa.

Phase	Pressure (GPa)	C_{11}	C_{12}	C_{13}	C_{22}	C_{23}	C_{33}	C_{44}	C_{55}	C_{66}
Fluorite phase	0	153.36	38.76					29.05		
	2	164.41	46.65					31.47		
	4	174.78	54.37					33.77		
	6	184.88	61.96					35.61		
	8	194.62	69.37					37.35		
$PbCl_2$-type phase	8	168.52	72.97	79.44	158.57	85.69	194.86	26.32	45.71	55.26
	10	177.50	81.46	86.25	171.10	94.32	208.49	28.26	49.48	58.88
	20	212.00	123.48	118.20	224.33	135.30	269.53	47.35	63.49	76.73
	30	239.37	165.51	148.63	273.93	171.22	324.00	61.62	74.74	92.96
	40	263.24	207.44	179.34	321.49	205.26	375.62	75.36	83.83	111.59
	50	276.95	249.88	208.27	369.14	238.05	425.16	87.42	92.55	125.49
	60	273.31	292.43	238.08	424.94	270.26	472.46	101.81	101.88	138.82
	70	268.64	316.20	261.00	497.42	310.24	516.53	119.56	112.15	137.78
	80	351.14	325.57	274.03	554.68	354.48	555.88	133.42	116.88	134.14
	90	431.68	343.17	283.53	601.03	401.73	590.69	147.37	119.27	137.07
	100	513.03	360.24	295.69	641.78	448.32	626.55	161.19	121.40	139.06
	110	592.50	380.80	304.63	678.88	499.04	655.93	173.98	122.08	142.36
	111.4	605.24	382.48	307.55	683.19	506.06	662.67	176.01	123.06	143.56
Ni_2In-type phase	111.4	742.52	511.53	285.58			796.50	119.83		115.50
	120	787.77	535.83	302.09			850.05	124.44		125.97
	130	839.67	563.79	319.67			910.80	127.60		137.94
	140	891.28	591.96	338.77			972.86	132.36		149.66
	150	943.59	619.53	357.03			1035.1	136.23		162.03

Furthermore, the elastic constants under different pressures calculated by GGA-PBE are listed in Table 4. The results as a function of pressure are also shown in Fig. 5 and Fig. 6. In Table 4, it is found that in the $PbCl_2$-type phase, C_{33} is larger than C_{11} and C_{22} when the pressure of 8 GPa–80 GPa, while C_{22} becomes the largest one when the pressure increase to 90 GPa. This result indicates that from 8 GPa to 80 GPa, the $PbCl_2$-type structure is more elastic along c axis than a and b axes, but the crystal is more difficult to compress along c axis when pressure larger than 90 GPa, which is consistent with the crystal constants shown in Fig. 4. From Fig. 5, we can see that C_{11}, C_{12}, and C_{44} in three phases increase linearly with pressure, except the C_{11} at 60 GPa–70 GPa. Because that C_{11} represents the compressibility along x direction, the CaF_2 crystal is easier to compress along the x axis in the pressure range of 60 GPa–70 GPa, which is consistent with the behavior of a/a_0 in Fig. 4.

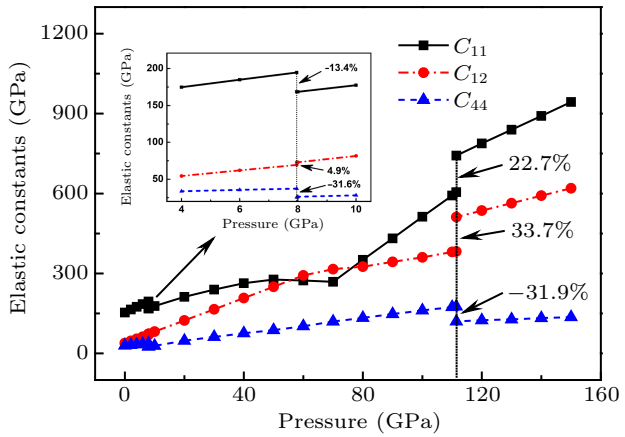


Fig. 5. Pressure dependence of elastic constants C_{11}, C_{12}, and C_{44} for three different phases calculated by GGA, the inserted picture emphasizing that value at 4 GPa–10 GPa.

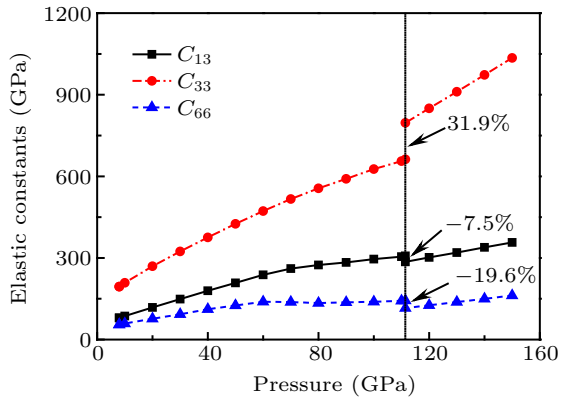


Fig. 6. Pressure dependence of elastic constants C_{13}, C_{33}, and C_{66} for $PbCl_2$-type and Ni_2In-type structures calculated by GGA.

Elastic constants are important tools for judging mechanical stability of crystal. It is necessary to analyze the mechanical stability of CaF_2 during the second-order phase transition because the independent elastic constants of three phases in CaF_2 crystal are related to the second-order change in the internal energy of a crystal under deformation. Generally, the mechanical stability can be evaluated by Born description, in which the elastic stability criteria are given below.[54]

For fluorite structure (cubic crystal),

$$C_{44} > 0, \quad C_{11} - C_{12} > 0, \quad C_{11} + 2C_{12} > 0. \tag{4}$$

For $PbCl_2$-type structure (orthorhombic crystal),

$$C_{11} > 0, \quad C_{11}C_{22} > C_{12}^2, \quad C_{44} > 0, C_{55} > 0, \quad C_{66} > 0,$$
$$C_{11}C_{22}C_{33} + 2C_{12}C_{13}C_{23} - C_{11}C_{23}^2 - C_{22}C_{13}^2 - C_{33}C_{12}^2 > 0. \tag{5}$$

And for Ni_2In-type structure (hexagonal crystal),

$$C_{11} > |C_{12}|, \quad 2C_{13}^2 < C_{33}(C_{11} + C_{12}), \quad C_{44} > 0, C_{66} > 0. \tag{6}$$

From Table 4, it is easy to see that in fluorite phase, C_{ij} are all larger than zero, and C_{11} are always larger than C_{12} from 0 GPa to 8 GPa, so the formula (4) is true. Similarly, we use formulas (5) and (6) to calculate the $PbCl_2$-type and Ni_2In-type structures, respectively and find that two phases satisfy the Born elastic stability criteria, which confirms the reliability of the second-order phase transition. However, Born stability conditions are not suggested to use at high pressures, and the stability criteria need to be reformulated at none-zero stress case. So far, there are different ways for how to use elastic constants to judge mechanical stability of crystal under high pressure. One of them is given by Sin'ko and Smirnov, they discussed this problem and told these conditions.[55,56]

For fluorite structure (cubic crystal),

$$(C_{11} - P) > 0, \quad (C_{44} - P) > 0,$$
$$(C_{11} - P) > |C_{12} + P|, \quad (C_{11} + 2C_{12} + P) > 0. \tag{7}$$

For $PbCl_2$-type structure (orthorhombic crystal),

$$(C_{11} - P) > 0, \quad (C_{22} - P) > 0, \quad (C_{33} - P) > 0.$$
$$(C_{44} - P) > 0, \quad (C_{55} - P) > 0, \quad (C_{66} - P) > 0,$$
$$(C_{11} + C_{22} - 2C_{12} - 4P) > 0, \quad (C_{11} + C_{33} - 2C_{13} - 4P) > 0,$$
$$(C_{22} + C_{33} - 2C_{23} - 4P) > 0,$$
$$(C_{11} + C_{22} + C_{33} + 2C_{12} + 2C_{13} + 2C_{23} + 3P) > 0. \tag{8}$$

For Ni_2In-type structure (hexagonal crystal),

$$(C_{11} - P) > 0, \quad (C_{33} - P) > 0, \quad (C_{44} - P) > 0,$$
$$(C_{11} - P) > |C_{12} + P|,$$
$$(C_{11} + C_{12})(C_{33} - P) > 2(C_{13} + P)^2. \tag{9}$$

The stability criteria of "$C_{11} + 2C_{12} + P$" of fluorite structure, and that of "$(C_{11} + C_{22} + C_{33} + 2C_{12} + 2C_{13} + 2C_{23} + 3P)$" of $PbCl_2$-type structure, always increase with the pressure. In addition, it is obvious that the stability criteria of "$(C_{11} + C_{12})(C_{33} - P) > 2(C_{13} + P)^2$" of Ni_2In-type structure

are true from Table 4. Thus, we presented the other stability criteria with applied pressure in Figs. 7 and 8. From Fig. 7, we can see that most of the mechanical stability criteria are satisfied, except that C_{44}–P in Ni_2In-type structure is slightly smaller than 0. In Fig. 8, the other four criteria are shown, in which M1 to M4 are $C_{11}+C_{22}-2C_{12}-4P$, $C_{11}+C_{33}-2C_{13}-4P$, $C_{22}+C_{33}-2C_{23}-4P$ of the $PbCl_2$-type structure and $C_{11}+C_{12}-2P$ of fluorite and Ni_2In-type structures, respectively. M4 is always larger than 0, while M1 and M2 decrease quickly with pressure and become negative at about 41 GPa and 66 GPa, respectively, and then increase from 80 GPa. On the other hand, M3 is slow down with increasing pressure before 70 GPa, but it drops sharply after that pressure. These sudden changes of M1 to M3 in $PbCl_2$-type structure at 70 GPa–80 GPa suggest the deformation of the structure, which is consistent with the changes of crystal constants b and c in Fig. 4. The stability criteria are also calculated by LDA, and the results are quite similar to the ones by GGA (not shown here).

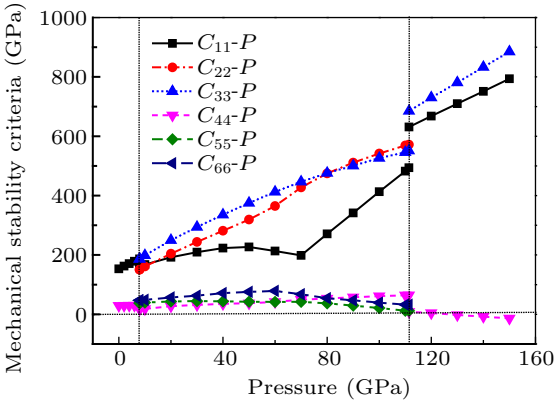


Fig. 7. Stability conditions C_{ii}–P as a function of pressure for three structures of CaF_2.

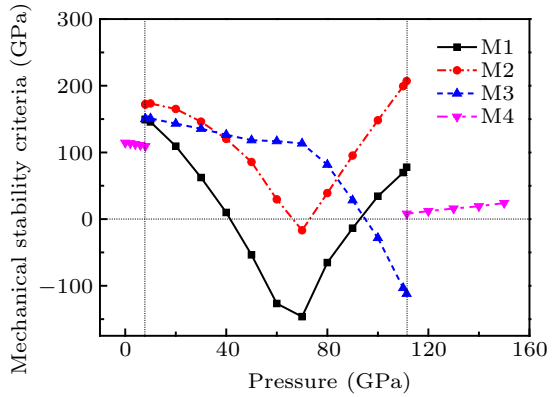


Fig. 8. Parts of stability conditions as a function of pressure for three structures of CaF_2.

To further study the mechanical properties of CaF_2 under pressures, we calculated the bulk modulus B, shear modulus G, and Young's modulus E with pressure with two kinds of exchange correlation-potential GGA-PBE and LDA-CAPZ, and the ratios B/B_0, G/G_0, and E/E_0 are shown in Fig. 9. The changes of these three ratios are also marked out at the critical pressure. Form the curves we can see that with pressure increase, all three modulus increase almost linearly, except for the pressure range of 60 GPa–80 GPa. Besides, the ratio B/B_0 grows faster than G/G_0 and E/E_0 obviously. It is known that Young's modulus E is the ratio of the pressure along an axis over the strain along that axis in the range of pressure, so the increasing of Young's modulus E with pressure gradually in Fig. 9 shows that the high-pressure phase of Ni_2In-type structure has better stiffness in CaF_2 crystal.

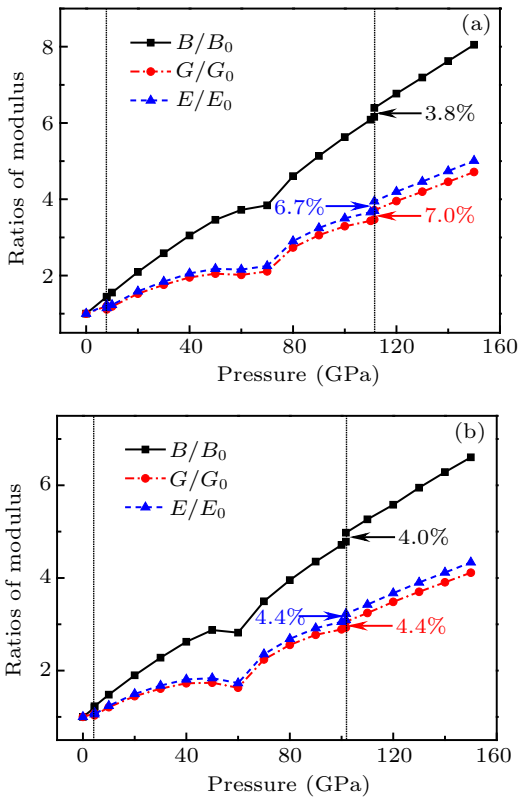


Fig. 9. Calculated ratios of bulk modulus B/B_0, shear modulus G/G_0, and Young's modulus E/E_0 as a function of pressure by both (a) GGA and (b) LDA.

It is well known that the Poisson's ratio v is always related to the mechanics of the crystal under pressure. A larger value of v usually means good ductility, and a smaller v is the opposite.[57] For central force solids, which have the best ductility, the value is between 0.25 and 0.5. Bur for ionic materials, the property of ductility is worse and the ratio of v is about 0.25. For the covalent materials, the ratio of v is most small (about 0.1).[58] The calculated Poisson's ratio v with exchange–correlation potentials GGA and LDA as a function of pressure is shown in Fig. 10 (black curves on the left). At the ground state, the ratio v is about 0.28–0.3, and it increases quickly with pressures. At the middle-pressure phase, this ratio continues to increase with pressure and reaches the maximum of about 0.38 at 60 GPa, but then decreases. At the

high-pressure phase of Ni_2In-type structure, the Poisson's ratio v maintains 0.36–0.37 and has hardly changes, indicating a high-pressure phase shows more ionic features than the ground state in its interatomic interactions.

Besides, the ratio of bulk modulus and shear modulus B/G is related to the nature of the compound: hardness or brittle. The key criterion was defined by Pugh:[59] when B/G is greater than 1.75, the compound is generally ductile; while when the ratio is less than 1.75, the compound is brittle. In this part, we calculate the ratio B/G of CaF_2 from 0 GPa to 150 GPa by both GGA and LDA, and also plot this ratio with the pressure increase in Fig. 10 (blue curves on the right). It can be found that the curves of B/G with increasing pressure are quite like the ones of ratio v, indicating that both two ratios relate to materials' mechanical properties. More importantly, the ratio B/G is always smaller than 1.75 in all of three phases and is larger in high-pressure phase than ground state, which indicates that better ductility can be anticipated for CaF_2 under high pressures. Moreover, the curves have obvious raises in the critical pressure between fluorite and $PbCl_2$-type structures, while the raises in the critical pressure between $PbCl_2$-type and Ni_2In-type structures are much smaller, suggesting the hardness of the material does not change too much in the second phase transition.

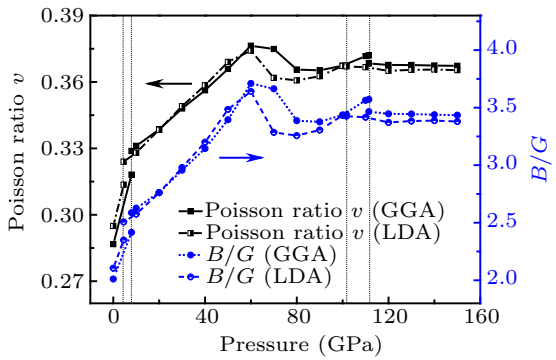


Fig. 10. Poisson ratio v and ratio B/G of CaF_2 with increasing pressures.

Debye temperature, correlating with specific heat, elastic constants, and melting temperature, is a fundamental parameter for material' thermodynamic properties. When the temperature is much higher than the Debye temperature, the heat capacity of the solid follows the classic law, *i.e.*, Dulong–Petit's law. Conversely, when the temperature is much lower than the Debye temperature, the heat capacity will follow the quantum law. Generally, we can theoretically obtain the Debye temperature using the following equation:[60]

$$\Theta_{\mathrm{D}} = \frac{h}{k}\left(\frac{3n}{4\pi}\frac{N\rho}{M}\right)^{1/3} v_{\mathrm{m}}, \tag{10}$$

where h, k, and N are the Planck's constant, Boltzmann's constant, and Avogadro constant, respectively. n is the atom number per molecule and M is the molecular weight. v_{m} is the average sound velocity, which can be calculated as

$$v_{\mathrm{m}} = \left[\frac{1}{3}\left(\frac{2}{v_{\mathrm{s}}^3} + \frac{1}{v_{\mathrm{p}}^3}\right)\right]^{-1/3}, \tag{11}$$

where v_{p} and v_{s} are the sound velocities for longitudinal and shear wave and can be described as

$$v_{\mathrm{p}} = \left[\frac{B+(4G/3)}{\rho}\right]^{1/2}, \quad v_{\mathrm{s}} = \left(\frac{G}{\rho}\right)^{1/2}, \tag{12}$$

where ρ denotes the density. B and G are bulk modulus and shear modulus, respectively. In this part, Debye temperature Θ_{D} and the average sound velocity v_{m} are both calculated by two exchange–correlation potentials with increasing pressures, and the results are shown in Fig. 11. We can see that with increasing pressure, Debye temperature Θ_{D} and average sound velocity v_{m} increase almost linearly except for the pressure range of 50 GPa–70 GPa, and these two values in high-pressure phases are much larger than that in low-pressure phases. In Debye theory, the Debye temperature Θ_{D} is the highest temperature of a crystal formed by a single normal vibration. In addition, the abnormal behavior in 50 GPa–70 GPa is related to the changes of the atom position in CaF_2, which is consistent with the behavior of crystal constants (Fig. 4) and mechanical properties (Figs. 9 and 10).

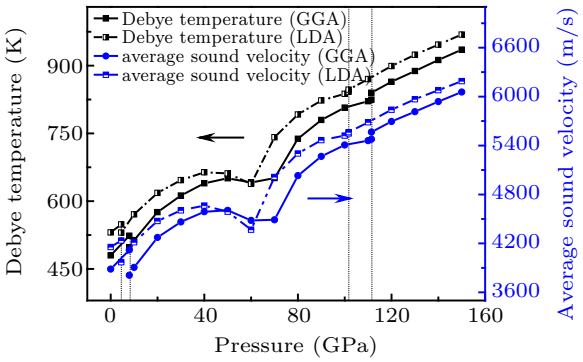


Fig. 11. Debye temperature Θ_{D} and average sound velocity v_{m} as a function of pressures calculated by GGA and LDA.

3.3. Electronic structure

In this part, we begin to investigate the pressure effects on the electronic structure of CaF_2 by analyzing the variation trend of the density of states (DOS) and band structure under pressures. Firstly, the band gaps of CaF_2 calculated by both GGA and LDA as a function of pressures are shown in Fig. 12. Generally, the band gap is always an important parameter to characterize the electronic structure of crystal. From Fig. 12, we can see that at the ground-state phase, the band gap increases quickly from about 7 eV to 7.6 eV with pressures. At

the critical pressure of the first-order phase transition, the band gap increases to about 8 eV suddenly. Then, with the pressure increase at the $PbCl_2$-type phase, the band gap increases slowly and starts to decrease at 70 GPa, indicating the structure has changed around 60 GPa–80 GPa, which is consistent with the changes of crystal constants of *b* and *c* in Fig. 4. With the pressure increase, the band gap has hardly changes at the Ni_2In-type phase and keeps around 5.5 eV–6 eV. Throughout the calculated pressure range of 0 GPa–150 GPa, CaF_2 maintains good insulation property. Our results in this part are consistent with those in other literatures.[26]

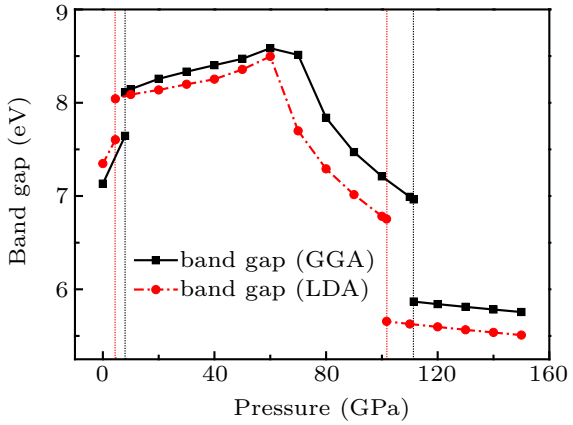


Fig. 12. The band gap of CaF_2 under different pressures.

Generally, with the increase of pressure in crystalline materials, the distances among atoms decrease, which leads to more overlap of the electron cloud and the tendency of ionic bonds transforming to covalent bonds. As a result, the band gap increases. On the other hand, when the pressure is large enough, some electrons no longer belong to one atom or one certain bond, those electrons become the so-called delocalized electrons. Such a phenomenon results in a reduction in the band gap. As far as we know, the research on the changes of band gap with pressure is basically a theoretical analysis, and it is only given in the experiment that the three phases of CaF_2 are insulators no matter under zero pressure or high pressure.[26] Figure 13 shows the charge density difference for fluorite structure along (111) plane at 0 GPa, which serves as a complementary tool for achieving a proper understanding of the electronic structure of the system CaF_2. From Fig. 13, we can conclude that there exists an ionic character along the Ca–F bond.

To further study the effect of pressure on the electronic structure of CaF_2, we investigated its total DOS and partial density of states (PDOS) by GGA. Figure 14 displays the DOS and PDOS of CaF_2 for fluorite structure at 0 GPa (Fig. 14(a)), $PbCl_2$-type structure at 8 GPa and 111.4 GPa (Figs. 14(b) and 14(c)), and Ni_2In-type structure at 111.4 GPa (Fig. 14(d)).

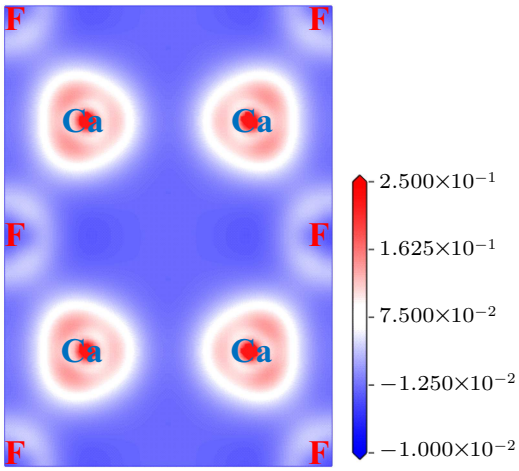


Fig. 13. Valence charge density difference (in units of $e/Å^3$) of fluorite structure along (111) plane at 0 GPa.

First, from Fig. 14(a), we can see that the peaks are independent near Fermi energy level and a gap more than 6 eV exists, indicating the CaF_2 crystal at zero GPa pressure is a type of insulator, which is corresponding with the band gap in Fig. 12. It is worth noting that some states crossing the Fermi energy is causing by the broadening of DOS. Besides, two strong peaks (about −1.2 eV and −2.4 eV) in the valence band occur below Fermi level, which are mainly contributed by 2p electronics in F atoms, indicating the F atoms obtaining most of the 3p electrons from Ca, and the characteristics of ionic crystal in CaF_2.

Then, from Figs. 14(b)–14(d), we can see that in $PbCl_2$-type and Ni_2In-type phases, the positions of two F atoms are not equivalent, which is different from the fluorite structure. In Fig. 14(b), the band gap is larger than that in Fig. 14(a), and the two nearly equal peaks in the valence band changed into one bigger than the others, which shows the locality of the $PbCl_2$-type phase of CaF_2. It also can be found that the DOS at 111.4 GPa (Fig. 14(c)) is wider than that at 8 GPa (Fig. 14(b)), which is due to the electrons' delocalization caused by pressures. The energy range covered under DOS curves is about −3.75 eV to 16.2 eV at 8 GPa, while the energy range is widened as about −6.5 eV to 18.3 eV at 111.4 GPa. For the valence band in PDOS, the highest two peaks shift from −1.2 eV and −2.4 eV towards negative energy levels of −2.3 eV and −4.3 eV, respectively. This phenomenon demonstrates that the covalent bonds form in deeper energy level under pressures, and bring strong bond strengths. It is obvious that at 111.4 GPa, the DOS of $PbCl_2$-type structure (Fig. 14(c)) is little different from that of Ni_2In-type structure (Fig. 14(d)): On the one hand, the valence band of CaF_2 in Ni_2In-type structure is slightly wider, and the two peaks are more independent. On the other hand, the band gap in Ni_2In-type structure reduces significantly.

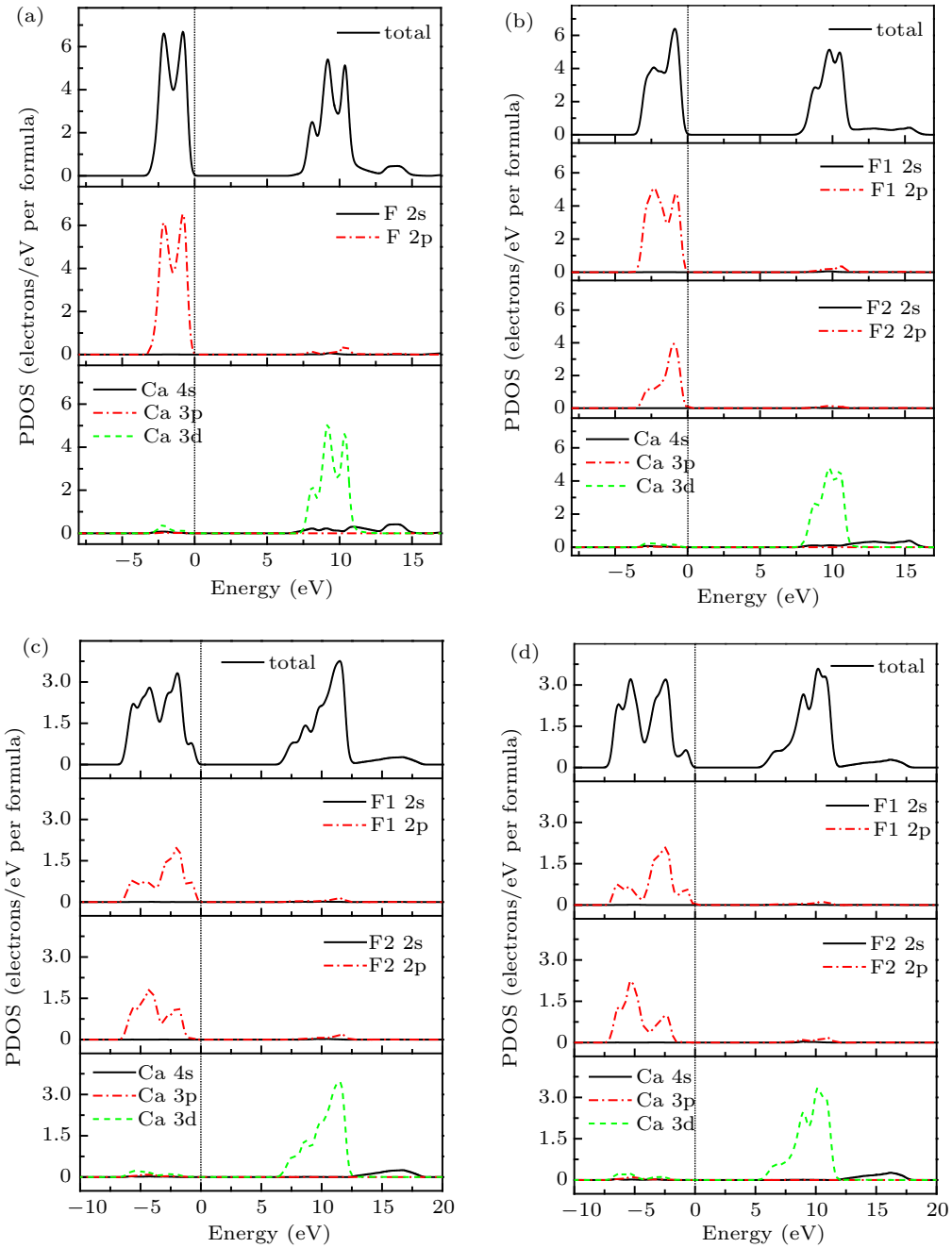


Fig. 14. DOS and PDOS of CaF_2 for fluorite structure at (a) 0 GPa, $PbCl_2$-type structure at (b) 8 GPa and (c) 111.4 GPa, and (d) Ni_2In-type structure at 111.4 GPa.

4. Conclusions

In conclusion, detailed DFT calculations of the structural, mechanical, thermodynamic, and electronic properties of crystalline CaF_2 with five different structures in the pressure range of 0 GPa–150 GPa are performed by both GGA-PBE and LDA-CAPZ, and the following results are obtained.

(i) The enthalpy difference implies that the fluorite phase $\rightarrow$ $PbCl_2$-type phase $\rightarrow$ Ni_2In-type phase transition in CaF_2 occurs at $P_{GGA1} = 8.0$ GPa, $P_{GGA2} = 111.4$ GPa by using the XC of GGA, and $P_{LDA1} = 4.5$ GPa, $P_{LDA2} = 101.7$ GPa by LDA, respectively. This result is consistent with previous experiments and theoretical conclusions.

(ii) The enthalpy differences between $PbCl_2$-type and Ni_2In-type phases in one molecular formula become very small at the pressure of about 100 GPa, indicating the possibility of coexistence of two phases at high pressures. This may be the reason why the transition pressure of the second phase transition in other reports is so huge (68 GPa–278 GPa).

(iii) The volume has hardly changed in the second phase transition, which is consistent with the approximately equal enthalpy of $PbCl_2$-type and Ni_2In-type phases at transition pressure.

(iv) The pressure dependence of mechanical and thermodynamic properties of CaF_2 are studied, and it is found that the high-pressure phase of Ni_2In-type structure has better stiff-

ness than that in CaF_2 crystal. Moreover, the ratio of B/G and Poisson's ratio v of CaF_2 has hardly changs in the second phase transition, suggesting the hardness of the material does not change too much in the second phase transition.

(v) The electronic structure of CaF_2 was also analyzed with the change of pressures. By analyzing the band gap and density of states, it is found that the CaF_2 crystal is always an insulator at 0 GPa–150 GPa.

References

[1] Dong Y J, Zhou G Q, Yang W Q, Su L B and Xu J 2004 *J. Inorg. Mater.* **19** 449 (in Chinese)
[2] Westerhoff T, Knapp K and Moersen E 1998 *Proc. SPIE* **3424** 10
[3] Rix S, Natura U, Loske F, Letz M, Felser C and Reichling M 2011 *Appl. Phys. Lett.* **99** 261909
[4] de Biasi R S and Grillo M L N 2012 *Physica B* **407** 2164
[5] Hazen R M and Finger L W 1981 *J. Appl. Crystallogr.* **14** 234
[6] Alzahrani A Z and Usanmaz D 2011 *J. Appl. Phys.* **109** 123708
[7] Muehlig C, Triebel W, Stafast H and Letz M 2010 *Appl. Phys. B* **99** 525
[8] Rubloff G W 1971 *Phys. Rev. B* **5** 662
[9] Barth J, Johnson R L, Cardona M, Fuchs D and Bradshaw A M 1990 *Phys. Rev. B* **41** 3291
[10] Gan F, Xu Y N, Huang M Z, Ching W Y and Harrison J G 1992 *Phys. Rev. B* **45** 8248
[11] Verstraete M and Gonze X 2003 *Phys. Rev. B* **68** 195123
[12] Shi H, Eglitis R I and Borstel G 2005 *Phys. Rev. B* **72** 045109
[13] Katrusiak A and Nelmes R J 1986 *J. Appl. Crystallogr.* **19** 73
[14] Angel R J 1993 *J. Phys.: Condens. Matter* **5** L141
[15] Angel R J, Allan D R, Miletich R and Finger L W 1997 *J. Appl. Crystallogr.* **30** 461
[16] Miletich R, Allan D R and Kuhs W F 2001 *Rev. Mineral. Geochem.* **41** 445
[17] Hu T J, Cui X Y, Wang J S, Zhang J K, Li X F, Yang J H and Gao C X 2018 *Chin. Phys. B* **27** 016401
[18] Seifert K F and Bunsenges B 1966 *Phys. Chem.* **70** 1041
[19] Dandekar D P and Jamieson J C 1969 *Trans. Am. Crystallogr. Assoc.* **5** 19
[20] Gerward L, Olsen J S, Steenstrup S, Åsbrink S and Waskowska A 1992 *J. Appl. Crystallogr.* **25** 578
[21] Speziale S and Duffy T S 2002 *Phys. Chem. Miner.* **29** 465
[22] Morris E, Groy T and Leinenweber K 2001 *J. Phys. Chem. Solids* **62** 1117
[23] El'kin F S, Tsiok O B, Khvostantsev L G and Brazhkin V V 2005 *J. Exp. Theor. Phys.* **100** 971
[24] Dorfman S M, Jiang F, Mao Z, Kubo A, Meng Y, Prakapenka V B and Duffy T S 2010 *Phys. Rev. B* **81** 174121
[25] Wang J S, Hao J, Wang Q S, Jin Y X, Li F F, Liu B, Li Q J, Liu B B and Cui Q L 2011 *Phys. Status Solidi B* **248** 1115
[26] Wu X, Qin S and Wu Z Y 2006 *Phys. Rev. B* **73** 134103
[27] Zeng Z Y, Chen X R, Zhu J and Hu C E 2008 *Chin. Phys. Lett.* **25** 230
[28] Cui S X, Feng W X, Hu H Q, Feng Z B and Wang Y X 2009 *Comp. Mater. Sci.* **47** 41
[29] Shi H, Luo W, Johansson B and Ahujia R 2009 *J. Phys.: Condens. Matter* **21** 415501
[30] Qi Y Y, Cheng Y, Liu M, Chen X R and Cai L C 2013 *Physica B* **426** 13
[31] Clark S J, Segall M D, Pickard C J, Hasnip P J, Probert M J, Refson K and Payne M C 2005 *Z. fuer Kristallogr.* **220** 567
[32] Segall M D, Lindan P J D, Probert M J, Pickard C J, Hasnip P J, Clark S J and Payne M C 2002 *J. Phys.: Condens. Matter* **14** 2717
[33] Laasonen K, Pasquarello A, Car R, Lee C and Vanderbilt D 1993 *Phys. Rev. B* **47** 10142
[34] Vanderbilt D 1990 *Phys. Rev. B* **41** 7892
[35] Liu L, Yi L, Liu H, Li Y, Zhuang C Q, Yang L X and Liu G P 2018 *Chin. Phys. B* **27** 047402
[36] Chen L M, Zhang K, Huang X, Zhang Y B, Xie Q Y and Li J 2020 *Int. J. Mod. Phys. C* **31** 2050025
[37] Huang D, Liu H, Hou M Q, Xie M Y, Lu Y F, Liu L, Li Y, Cui Y J, Li Y, Deng L W and Du J G 2017 *Chin. Phys. B* **26** 089101
[38] Chen L M, Zhang Y B, Zhang K, Huang X, Li J and Xie Q Y 2020 *Int. J. Mod. Phys. C* **31** 2050133
[39] Blanco M A, Francisco E and Luana V 2004 *Comput. Phys. Commun.* **158** 57
[40] Perdew J P, Burke K and Ernzerhof M 1996 *Phys. Rev. Lett.* **77** 3865
[41] Ceperley D M and Alder B J 1980 *Phys. Rev. Lett.* **45** 566
[42] Perdew J P and Zunger A 1981 *Phys. Rev. B* **23** 5048
[43] Kresse G and Furthmller J 1996 *Phys. Rev. B* **54** 11169
[44] Fletcher R 1980 *Practical Methods of Optimization* (New York: Wiley) p. 120
[45] Wevers M A C, Schon J C and Jansen M 1998 *J. Solid State Chem.* **136** 233
[46] Leger J M, Haines J, Atouf A, Schulte O and Hull S 1995 *Phys. Rev. B* **52** 13247
[47] Poirier P J 2000 *Introduction to the physics of the earth's interior* (C. U. Press)
[48] Pendás A M, Recio J M, Flórez M and Luaña V 1994 *Phys. Rev. B* **49** 5858
[49] Kanchana V, Vaitheeswaran G and Rajagopalan M 2003 *Physica B* **328** 283
[50] Ivanovskii A L 2012 *Prog. Mater. Sci.* **57** 184
[51] Barron T and Klein M 1965 *Proc. Phys. Soc.* **85** 523
[52] Wang J, Li J, Yip S, Phillpot S and Wolf D 1995 *Phys. Rev. B* **52** 12627
[53] Duane C W 1972 *American Journal of Physics* **40** 1718
[54] Mouhat F and Coudertlk F X 2014 *Phys. Rev. B* **90** 2241104
[55] Sin'ko G V and Smirnov N A 2002 *J. Phys.: Condens. Matter* **14** 6989
[56] Sin'ko G V. and Smirnov N A 2004 *J. Phys.: Condens. Matter* **16** 8101
[57] Schroers J and Johnson W L 2004 *Phys. Rev. Lett.* **93** 255506
[58] Santamaría-Pérez D, Kumar R S, Dos Santos-García A J, Errandonea D, Chuliá-Jordán R, Saez-Puche R, Rodríguez-Hernández P and Munoz A 2012 *Phys. Rev. B* **86** 94116
[59] Pugh S F 1954 *Philos. Mag.* **45** 823
[60] Grimvall G 1999 *Thermophysical Properties of Materials* (Amsterdam: Elsevier)